PCCP

Accepted Manuscript

ROYAL SOCIETY OF CHEMISTRY

www.rsc.org/pccp

Journal Name

RSCPublishing

ARTICLE

Separating Redox Couple for Highly Efficient Solid-State Dye-Sensitized Solar Cells

Cite this: DOI: 10.1039/x0xx00000x

Juan Li, Wei Zhang, Lu Zhang and Zhong-Sheng Wang*

Received 00th January 2012,
Accepted 00th January 2012

DOI: 10.1039/x0xx00000x

www.rsc.org/

To minimize the charge recombination between electron and electron acceptor in solid-state dye-sensitized solar cells, we propose separated electron donor and acceptor of a redox couple in the photoanode and on the cathode, respectively. Owing to the absence of acceptor in the photoanode initially, charge recombination rate is retarded remarkably, resulting in increased short-circuit photocurrent by > 2-fold, open-circuit photovoltage by 71 mV and power conversion efficiency by > 2.5-fold.

Introduction

Dye-sensitized solar cells (DSSCs) have been attracting considerable attention due to their potential low cost and high performance.[1] A typical DSSC comprises a dye-sensitized TiO_2 film as the photoanode, a platinized conductive glass as the cathode and a redox couple based electrolyte sandwiched between the two electrodes. The electron donor (e.g. I^-) in the electrolyte fulfils dye regeneration upon electron injection from the excited dye to the conduction band of TiO_2 while the electron acceptor (e.g. I_3^-) in the electrolyte accepts electrons at the cathode to complete the circuit.[2] However, the presence of I_3^- in the photoanode layer leads to charge recombination between electrons and I_3^-, resulting in drop of photovoltaic performance

In fact, the photoanode layer only needs the electron donor for fast dye regeneration, while the electron acceptor should locate at the surface of counter electrode for efficient electron relay to the internal of the device. If the electron acceptor is moved from the photoanode layer to the surface of counter electrode, the charge recombination between electrons and I_3^- can be minimized due to the absence of triiodide in the photoanode initially and meanwhile fast electron transfer from the cathode to the internal of the device can also be maintained. Unfortunately, the separation of donor and acceptor cannot be realized with the liquid electrolyte,[3] but it can be realized with the solid-state electrolytes for solid-state DSSCs (ssDSSCs).[4-8]

Herein, we prepared double-ester-substituted imidazolium iodide (DEII, Figure 1) to act as the electron donor. The donor was deposited in the dye-loaded TiO_2 layer for efficient dye regeneration preceded by electron injection from the excited dye to the conduction band of TiO_2, while the acceptor (mixture of DEII and iodine at a molar ratio of 6:1, or I^-/I_3^- = 5:1, the same below) was deposited on the cathode surface for efficient electron relay from the cathode to the inside of the cell for circuit completion. The cathode was placed on top of the photoanode to form a close contact between the donor and acceptor, which was then sealed into a solid device. As compared to the redox mixture electrolyte based device A (Scheme 1), separating the electron donor and acceptor of a redox couple in device B (Scheme 1) could significantly retard charge recombination because of the absence of I_3^- in the photoanode initially. As a consequence, photovoltaic performance was improved remarkably.

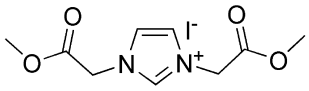

Figure 1. The chemical structure of DEII

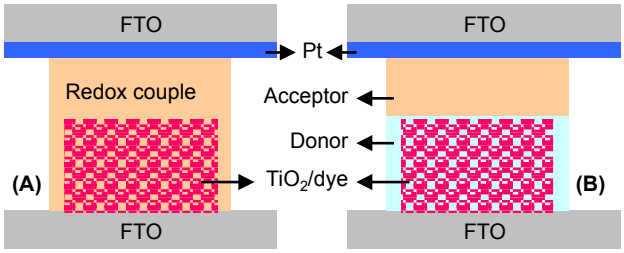

Scheme 1. The device structures for device A and device B. A redox-couple mixture is used as the solid-state electrolyte in device A while the electron donor and acceptor of the redox-couple are separated in device B: the donor is in the photoanode layer but the acceptor (the mixture of donor and acceptor) is on the top of photoanode in contact with the cathode.

Results and Discussion

The synthetic procedures of DEII are described in the Experimental Section. The chemical structure of DEII was corroborated with ^{1}H NMR, ^{13}C NMR and HRMS (Figure S1). The decomposition temperature (Figure S2) is 140 ^{o}C and the melting point (Figure S3) is 128 ^{o}C for DEII.

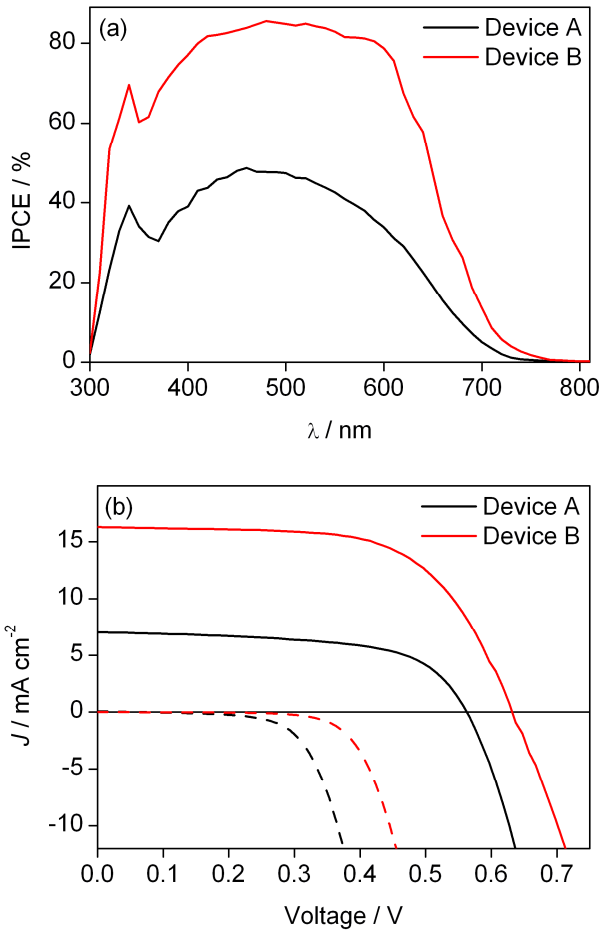

Figure 2. (a) IPCE spectra and (b) *J-V* curves for device A and B under simulated AM1.5G illumination and dark.

To highlight the advantage of separated donor and acceptor in the ssDSSC and exactly compare the solar cell performance arising from the photoanode part, the top acceptor layer above photoanode in device B is the DEII/I_2 mixture, which is the same as in device A. Figure 2a displays the incident monochromatic photon-to-electron conversion efficiency (IPCE) as a function of wavelength for the solid-state devices with 16-μm TiO_2 film[9] and a metal-free organic dye sensitizer[10] (Figure S4). In the visible spectral range, the IPCE values increases remarkably from device A to device B. This forebodes that device B can produce much higher photocurrent than device A. Figure 2b shows the *J-V* curves for device A and B under AM1.5G full-sun irradiation. Device A produces short-circuit photocurrent density (J_{sc}) of 7.02 mA cm^{-2}, open-circuit photovoltage (V_{oc}) of 562 mV and fill factor (FF) of 0.61, corresponding to power conversion efficiency (PCE) of 2.41%, while device B produces J_{sc} of 16.29 mA cm^{-2}, V_{oc} of 633 mV and FF of 0.63, corresponding to PCE of 6.50%. The J_{sc} increases by more than 2-fold from device A to device B, which is consistent with the IPCE result. In addition, the V_{oc} is improved by 71 mV from device A to device B. To compare the back-reaction with triiodide, *J-V* curves were measured under dark and are shown in Figure 2b. The onset potential of dark current shifted to higher value from device A to B, in good agreement with the variation of V_{oc}. As a result, the PCE is enhanced by more than 2.5-fold when the acceptor is removed from the photoanode layer but remained in the top layer. These data clearly support that separating electron donor and acceptor can improve photovoltaic performance remarkably.

4-tertbutylpyridine (TBP) is a typical additive in the electrolyte to suppress charge recombination. For comparison, we fabricated two reference devices with DEII/I_2/TBP (5:1/4) or DEII/I_2/LiI/TBP (5/1/0.5/4) as the electrolyte, respectively. The device with DEII/I_2/TBP produced J_{sc} of 11.01 mA cm^{-2}, V_{oc} of 743 mV and FF of 0.71, corresponding to PCE of 5.81%, and the device with DEII/I_2/LiI/TBP produced J_{sc} of 11.69 mA cm^{-2}, V_{oc} of 752 mV and FF of 0.68, corresponding to PCE of 5.98%. As compared to device B with separated donor and acceptor, the device with TBP yielded lower PCE despite the higher V_{oc} due to the much decreased photocurrent. This clearly indicates that our approach is better than simply adding TBP in terms of power conversion efficiency, although the electrolytes with TBP are not all-solid-state.

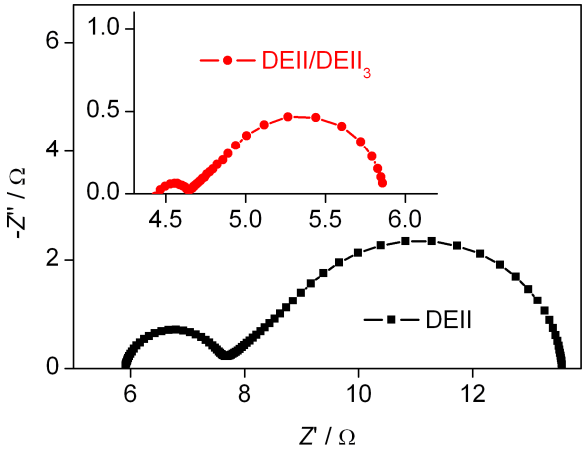

Figure 3. EIS Nyquist plot of dummy cells made of two identical platinized FTO substrates (active area of 0.35 cm^2, distance of 30 μm) sandwiched with DEII or the DEII/I_2 mixture (inset)

The ionic conductivity of solid electrolyte is an important factor in determining photovoltaic performance of ssDSSCs. Figure 3 shows the electrochemical impedance spectroscopy of dummy cells sandwiched with solid DEII or the DEII/I_2 mixture. The left semicircle is attributed to the reduction of triiodide to iodide at the electrode/electrolyte interface. The radius of this semicircle on the real axis represents the resistance of charge transfer at the electrode/electrolyte

interface (R_{ct}). As much more triiodide exists in the DEII/I_2 mixture than in DEII, the former exhibits smaller R_{ct} than the latter. It is noted that very small amount of I_3^- (molar ratio of I_3^- /I^- = 4.9 × 10^{-4}) is contained in the solid DEII due to contamination (Figure S5). The right semicircle comes from the diffusion in the solid electrolyte between electrodes. The diameter of this semicircle on the real axis is used to estimate the ionic conductivity of the solid electrolyte. DEII and the DEII/I_2 mixture exhibit ionic conductivity at RT of 1.5 and 7.0 mS cm^{-1}, respectively. The conversion of iodide to triiodide results in significant reduction of the distance between adjacent iodides, which makes Grotthus charge exchange[11] along the iodide chain more efficient and accounts for the higher ionic conductivity for the DEII/I_2 mixture.

Ionic movements of iodide and triiodide via Grotthus charge exchange for both DEII and the DEII/I_2 mixture are characterized by linear sweep voltammogram (LSV) on dummy cells sandwiched with solid DEII or the DEII/I_2 mixture.[12] The LSV curves of DEII and the DEII/I_2 mixture show plateau of limiting current at a slow san rate (10 mV s^{-1}), as shown in Figure 4, which is controlled by the ionic movement via Grotthus charge exchange. As the limiting current density is proportional to the concentration of triiodide due to the large excess of iodide, the DEII/I_2 mixture produces much higher limiting current density than DEII.[7]

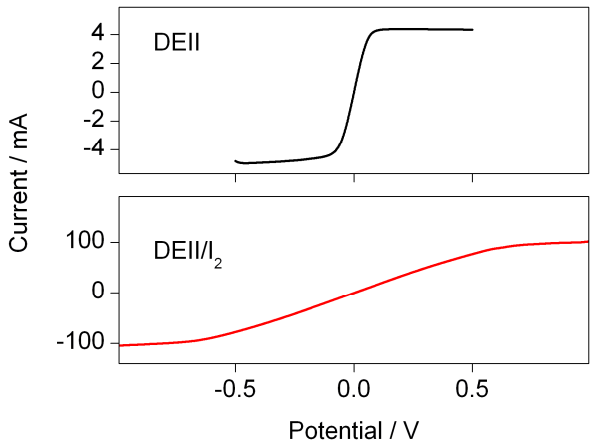

Figure 4. LSV curves for the dummy cells made of two identical platinized FTO substrates (active area of 0.35 cm^2, distance of 30 μm) sandwiched with DEII or the DEII/I_2 mixture

The electron transfer in device B is similar to that in device A that contains a typical redox couple based electrolyte in one phase. Upon electron injection from the excited dye to the conduction band of TiO_2, the electron donor (I^-) in DEII is oxidized by dye cation and changes to the electron acceptor (I_3^-), which moves quickly via Grotthus charge exchange to the donor/acceptor interface, due to the high ionic conductivity and limiting current of DEII, and then to the counter electrode through the top acceptor layer. The electron acceptor (I_3^-) deposited on the surface of cathode accepts electron and changes to the donor (I^-), which moves quickly via Grotthus charge exchange to the donor/acceptor interface and then to the photoanode layer. A close contact between donor and acceptor layers ensures fast interfacial charge transfer.

As the top electrolyte part is same for both devices while the bottom electrolyte part in the photoanode layer for device A has higher ionic conductivity or limiting current density than that for device B, device A should generate better photovoltaic performance without taking other factors into account. However, device B produces higher J_{sc}, V_{oc} and PCE than device A. This indicates that there is another factor influencing the solar cell performance significantly.

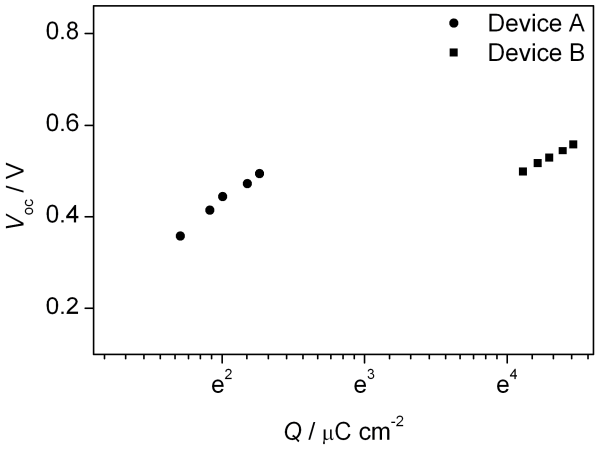

Figure 5. Relationship between V_{oc} and charge density

The V_{oc} depends on the conduction band (CB) edge of TiO_2 and free electron density in the CB.[13] Figure 5 shows the plot of charge density (Q) at open circuit against open-circuit photovoltage under LED light with various intensities. For both device A and device B, the V_{oc} increases with the logarithm of charge density, and the slope is almost the same (170 mV). As compared to device A with the mixture electrolyte, the separation of the donor and acceptor shifts the CB edge positively by 280 mV, as seen from Figure 5.[13] As compared to device A, the positive shift of CB for device B is beneficial for higher electron injection yield and hence photocurrent generation. The observed higher J_{sc} for device B can be explained by the relative lower CB. The concentration gradient of I_3^- from photoanode to counter electrode is also advantageous to improving the photovoltaic performance as reported by Hayase et al.[14] However, the positive shift of CB should lead to a decrease in V_{oc}, contrasting to the observed higher V_{oc}. This suggests that separation of the donor and acceptor in device B should suppress charge recombination.

As I_3^- is initially absent in the photoanode layer of device B while large amount of I_3^- is present in the photoanode layer of device A, the two devices should have different charge recombination rate between electrons and I_3^-. To verify this point, electron lifetime was measured with intensity modulated photovoltage spectra (IMVS) under LED green light (532 nm) with various intensities. Figure 6 shows the relationship

between electron lifetime and charge density obtained from charge extraction. Electron lifetime is enhanced by more than three orders of magnitude from device A to device B at the same charge density. This indicates that charge recombination between electrons and triiodide is retarded remarkably when the device structure is changed from A to B. As compared to device A, the higher electron lifetime in device B is attributed to the absence of triiodide in the photoanode layer initially as the electron lifetime is expected to increase with decreasing the acceptor concentration.[15] The remarkable increase in electron lifetime brings about more electrons stored in TiO_2, resulting in significant improvement of V_{oc} from device A to B.[16] The charge densities, which depend on the photo-injected electron density and electron lifetime at open-circuit, are measured of 10 and 85 μC cm^{-2} under 45 W cm^{-2} LED light (532 nm) for device A and device B, respectively. It is derived from Figure 5 that V_{oc} gain solely arsing from the increased charge density is about 360 mV. Therefore, the collective effects of the positively shifted CB edge (280 mV) and the increased charge density contribute to an increase in V_{oc} by 80 mV, which is in agreement with the observed increase in V_{oc} under the same LED light.

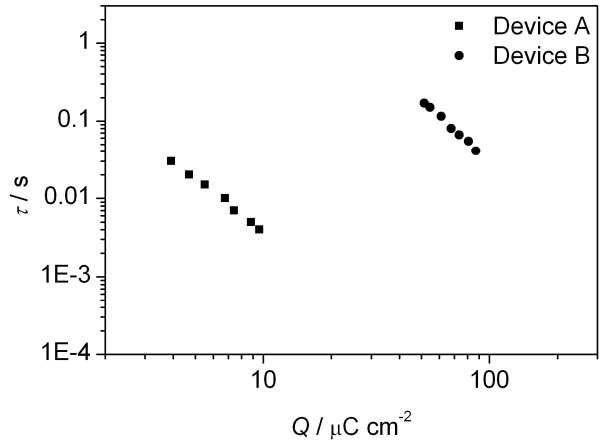

Figure 6. Relationship between electron lifetime and charge density

Conclusions

In summary, we demonstrate the separation of redox couple in the ssDSSC device and its advantage over the mixed redox-couple electrolyte for the first time. Contrasting to the redox-couple based solid electrolyte, moving the electron acceptor from the photoanode to cathode can inhibit charge recombination remarkably due to the absence of triiodide in the photoanode layer initially and meanwhile shift the CB edge positively. As a consequence, J_{sc}, V_{oc} and PCE are improved remarkably upon separation of the donor and acceptor of the redox couple. With the new device structure, photovoltaic performance can be further optimized by increasing the ionic conductivity of the electron donor through molecular design.[17] This new device structure opens up a new way for optimization of solar cell performance.

Experimental Section

Synthesis of 1-(2-methoxy-2-oxoethyl)imidazole. Absolute dry methanol (50 mL) and sodium (2.3 g, 0.1 mol) were charged into a 100 mL three-necked flask equipped with a condensing tube and stirred at RT for 2 h. Then imidazole (6.8 g, 0.1 mol) was added to the above mixture, which was heated to 50 °C and stirred for 1 h followed by addition of methyl chloroacetate (21.7 g, 0.2 mmol). The reaction was kept at 50 °C for additional 16 h. After the solid was filtrated, the solvent was removed via rotary evaporation until yellow oil remained. Silica gel chromatography with CH_2Cl_2:CH_3OH (20:1, volume ratio) as eluent afforded the pure product as a white solid (yield, 67.0%). ^{1}H-NMR ($CDCl_3$, 400 Hz, δ ppm): 7.87 (s, 1H); 7.11 (s, 1H); 6.87 (s, 1H), 4.94 (s, 2H); 3.66 (s, 3H). ^{13}C-NMR (DMSO-d_6, 50 MHz, δ ppm): 168.2, 138.3, 129.8, 120.2, 53.1, 48.0.

Synthesis of methyl 2-iodoacetate (ICH_2COOCH_3). 1 equiv. methyl 2-chloroacetate (3.472 g, 32 mmol) and 10 equiv. NaI (48 g, 320 mmol) were dissolved in 250 mL acetone and the mixture was stirred at RT for 72 h under nitrogen atmosphere. The solvent was evaporated and the product was dissolved in CH_2Cl_2. The precipitated sodium chloride was filtrated off. Evaporation of CH_2Cl_2 yielded 2-iodoacetate (yield, 90%). ^{1}H-NMR ($CDCl_3$, 400 Hz, δ ppm): 3.69~3.71 (s, 3H); 3.63~3.68 (s, 2H).

Synthesis of 1,3-di(2-methoxy-2-oxoethyl)imidazolium iodide (DEII). 1.5 equiv. 2-iodoacetate (3 g, 15 mmol) and 1-(2-methoxy-2-oxoethyl) imidazole (1.4 g, 10 mmol) were dissolved in 10 mL CH_3Cl_3 and the mixture was stirred at 60 °C for 48 h. The product was washed with diethyl ether, affording pale yellow solid product (yield, 95%). ^{1}H-NMR (DMSO-d_6, 400 Hz, δ ppm): 9.114 (s, 1H); 7.763 (s, 2H); 5.316 (s, 4H); 3.731 (s, 6H). ^{13}C-NMR (DMSO-d_6, 50 MHz, δ ppm): 167.9, 139.1, 124.3, 53.6, 50.5, 39.6~40.8. HRMS (ESI, m/z): $[M+H]^+$ calcd for $C_9H_{13}N_2O_4$, 213.0875; found 213.0877.

Solar Cell Fabrication and Solar Cell Performance Measurements. TiO_2 films (15 μm) composed of a 10 μm nanoparticle (20 nm) layer in direct contact with the FTO substrate and 5 μm light scattering particle (80% 20 nm TiO_2 + 20% 100 nm TiO_2) layer were sintered at 525 °C for 2 h to achieve good necking of neighboring TiO_2 particles under an airflow. Film thickness was measured with a surface profiler (Veeco Dektak 150, USA). Sintered films were then treated with 0.05 M $TiCl_4$ aqueous solution at 70 °C for 30 min and then rinsed with deionized water. The $TiCl_4$-treated TiO_2 films were annealed at 450 °C for 30 min and then cooled to 120 °C before immersing into the dye (Figure S4) solution (0.3 mM in toluene) for 16 h at room temperature for complete dye adsorption. For device A, dye-loaded TiO_2 film as the working electrode and the Pt-coated FTO as the counter electrode were separated by a hot-melt Surlyn film (30 μm) and sealed together by pressing them under heat. The methanol solution of the mixture electrolyte was injected into the internal space of the cell from the two holes predrilled on the back of the counter electrode and dried on a hot plate at 50 °C until the TiO_2 porous

film was filled with the solid-state electrolyte. For device B, the methanol solution of DEII was dropped onto the dye-loaded TiO_2 film and dried on a hot plate at 50 °C until the TiO_2 porous film was filled with DEII. The methanol solution of the DEII/I_2 mixture (molar ratio 5:1) was drop-casted onto the surface of counter electrode and dried on a hot plate at 50 °C. The counter electrode deposited with the DEII/I_2 mixture was placed on top of the working electrode filled with DEII and assembled together. The two cells were further dried in a vacuum oven at 50 °C for 2 days to completely remove the residual methanol before sealing. The working performance of DSSC was tested by recording the current density−voltage (*J*−*V*) curves with a Keithley 2400 Source Meter (Oriel) under illumination of simulated AM1.5G solar light coming from an AAA solar simulator (Newport-94043A) equipped with a Xe lamp (450 W) and an AM1.5G filter. Light intensity was calibrated using a standard Si solar cell (Newport 91150) equipped with a KG-5 filter. Action spectra of incident mono-chromatic photon-to-electron conversion efficiency (IPCE) as a function of wavelength were obtained on an Oriel-74125 system (Oriel Instruments). The intensity of incident monochromatic light was measured with a Si detector (Oriel-71640). A black mask with an aperture area of 0.2304 cm^2 was used during measurement to avoid stray light completely.

Characterizations. The chemical structure was characterized by ^{1}H NMR (), ^{13}C NMR (Varian 400 MHz NMR spectrometer) and HRMS (HP-5988A). Thermo gravimetric (TG) analysis was performed on a TG-DTA 2000S system (Mac Sciences Co. Ltd., Yokohama, Japan) at a heating rate of 10 °C min^{-1}. Differential scanning calorimetry (DSC) was performed on a DSC 822e thermal analysis system (Mettler Toledo Instruments Inc., Switzerland) with nitrogen gas as purge (80 mL min^{-1}) at a heating rate of 5 °C min^{-1}. UV−vis absorption spectra were scanned on a UV−vis−NIR spectrophotometer (Shimadzu UV-2550) in transmission mode. Solid-state electrolytes were sandwiched in dummy cells between two identical Pt electrodes, which were used for measurements of electrochemical impedance spectroscopy (EIS) in a frequency range from 1 Hz to 10^5 Hz and linear sweep voltammetry (LSV) on an electrochemical workstation (Zahner XPOT, Germany). The electron lifetimes were measured with controlled intensity modulated photovoltage spectroscopy (IMVS), and charge densities at open circuit were measured using charge extraction technique. IMVS and charge extraction analysis were carried out on an electrochemical workstation (Zahner XPOT), which includes a green light-emitting diode (LED, 532 nm) and the corresponding control system. The intensity-modulated spectra were measured at room temperature with light intensity ranging from 0.5 to 45 $W.m^{-2}$, in modulation frequency ranging from 0.1 Hz to 10 kHz, and with modulation amplitude less than 5% of the light intensity.

Acknowledgements

This work was financially supported by National Basic Research Program (2011CB933302) of China, STCSM (12JC1401500) and Jiangsu Major Program (BY2010147).

Notes and references

Department of Chemistry, Lab of Advanced Materials, Collaborative Innovation Center of Chemistry for Energy Materials, Fudan University, 2205 Songhu Road, Shanghai 200438, P. R. China. Email: zs.wang@fudan.edu.cn

† Footnotes should appear here. These might include comments relevant to but not central to the matter under discussion, limited experimental and spectral data, and crystallographic data.

Electronic Supplementary Information (ESI) available: [details of any supplementary information available should be included here]. See DOI: 10.1039/b000000x/

1 (a) B. O'Regan and M. Grätzel, *Nature*, 1991, **353**, 737.; (b) Y. Bai, Y. Cao, J. Zhang, M. Wang, R. Li, P. Wang, S. M. Zakeeruddin and M. Grätzel, *Nat. Mater.,* 2008, **7**, 626; (c) P. Wang, S. M. Zakeeruddin, J. E. Moser, M. K. Nazeeruddin, T. Sekiguchi and M. Grätzel, *Nat. Mater.,* 2003, **7**, 402.

2 A. Hagfeldt, G. Boschloo, L. Sun, L. Kloo and H. Pettersson, *Chem. Rev.*, 2010**, 110***,* 6595.

3 H. Tian, X. Jiang, Z. Yu, L. Kloo, A. Hagfeldt and L. Sun, *Angew. Chem. Int. Ed*., 2012, **49**, 7328.

4 J. Shi, L. Wang, Y. Liang, S. Peng, F. Cheng and J. Chen, *J. Phys. Chem. C*, 2010, **114***,* 6814.

5 N. Yamanaka, R. Kawano, W. Kubo, N. Masaki, T. Kitamura, Y. Wada, M. Watanabe and S. Yanagida, *J. Phys. Chem. B*, 2007, **111***,* 4763.

6 A. Midya, Z. B. Xie, J. X. Yang, Z. K. Chen, D. J. Blackwood, J. Wang, S. Adama, K. P. Loh, *Chem. Commun*., **2010**, *46*, 2091.

7 (a) H. Wang, X. Zhang, F. Gong, G. Zhou and Z.-S. Wang, *Adv. Mater.*, 2012, **24**, 121; (b) W. Zhang, J. Li, S. H. Jiang and Z.-S. Wang, *Chem. Comm.*, 2014, **50**, 1685; (c) J. Li, H. Wang, G. Zhou and Z.-S. Wang, *Chem. Comm.*, 2013, **49**, 9446.

8 Q. Li, J. Zhao, B. Sun, B. Li, L. Qiu, Y. Zhang, X. Chen, J. Lu, F. Yan, *Adv. Mater*., **2012**, *24*, 945.

9 Z.-S. Wang, H. Kawauchi, T. Kashima and H. Arakawa, *Coord. Chem. Rev.*, 2004, **248**, 1381.

10 Y. Li, H. Wang, Q. Feng, G. Zhou and Z.-S. Wang, *Energy Environ. Sci.*, 2013, **6**, 2156.

11 V. K. Thorsmølle, G. Rothenberger, D. Topgaard, J. C. Brauer, D.-B. Kuang, S. M. Zakeeruddin, B. Lindman, M. Grätzel and J.-E. Moser, *ChemPhysChem*, 2011, **12**, 145.

12 A. Hauch and A. Georg, *Electrochim. Acta* 2001, **46**, 3457.

13 G. Schlichthörl, S. Y. Huang, J. Sprague, A. J. Frank, *J. Phys. Chem. B*, 1997, **101**, 8141.

14 T. Kato and S. Hayase, *J. Electrochem. Soc.,* 2007, **154**, B117.

15 S. Nakade, T. Kanzaki, W. Kubo, T. Kitamura, Y. Wada and S. Yanagida, *J. Phys. Chem. B*, 2005, **109**, 3480.

16 F. Fabregat-Santiago, G. Garcia-Belmonte, I. Mora-Seró and J. Bisquert, *Phys. Chem. Chem. Phys*., 2011, **13**, 9083; (b) X. Zhang, Q. Huang, G. Zhou and Z.-S. Wang, *J. Phys. Chem. C*, 2011, **115**, 12665.

17 H. Wang, J. Li, F. Gong, G. Zhou and Z.-S. Wang, *J. Am. Chem. Soc.*, 2013, **135**, 12627.